



Reconstruction and analysis of the transmission network of African swine fever in People's Republic of China, August 2018–September 2019

Original Paper

Cite this article: Akhmetzhanov AR, Jung S-m, Lee H, Linton NM, Yang Y, Yuan B and Nishiura H (2024). Reconstruction and analysis of the transmission network of African swine fever in People's Republic of China, August 2018–September 2019. *Epidemiology and Infection*, **152**, e27, 1–9
<https://doi.org/10.1017/S0950268824000086>

Received: 01 September 2023

Revised: 14 December 2023

Accepted: 25 December 2023



Keywords:

African swine fever; animal pathogens; epidemics; mathematical modelling; veterinary epidemiology

Corresponding author:

Hiroshi Nishiura;

Email: nishiura.hiroshi.5r@kyoto-u.ac.jp

Andrei R. Akhmetzhanov^{1,2} , Sung-mok Jung², Hyojung Lee², Natalie M. Linton², Yichi Yang², Baoyin Yuan² and Hiroshi Nishiura^{3,4} 

¹Global Health Program & Institute of Epidemiology and Preventive Medicine, National Taiwan University College of Public Health, Taipei, Taiwan; ²Graduate School of Medicine, Hokkaido University, Sapporo, Japan; ³School of Public Health, Kyoto University, Kyoto, Japan and ⁴CREST, Japan Science and Technology Agency, Saitama, Japan

Abstract

Introduction of African swine fever (ASF) to China in mid-2018 and the subsequent trans-boundary spread across Asia devastated regional swine production, affecting live pig and pork product-related markets worldwide. To explore the spatiotemporal spread of ASF in China, we reconstructed possible ASF transmission networks using nearest neighbour, exponential function, equal probability, and spatiotemporal case-distribution algorithms. From these networks, we estimated the reproduction numbers, serial intervals, and transmission distances of the outbreak. The mean serial interval between paired units was around 29 days for all algorithms, while the mean transmission distance ranged 332–456 km. The reproduction numbers for each algorithm peaked during the first two weeks and steadily declined through the end of 2018 before hovering around the epidemic threshold value of 1 with sporadic increases during 2019. These results suggest that 1) swine husbandry practices and production systems that lend themselves to long-range transmission drove ASF spread; 2) outbreaks went undetected by the surveillance system. Efforts by China and other affected countries to control ASF within their jurisdictions may be aided by the reconstructed spatiotemporal model. Continued support for strict implementation of biosecurity standards and improvements to ASF surveillance is essential for halting transmission in China and spread across Asia.

Introduction

African swine fever (ASF) is a highly contagious and fatal disease of domestic pigs and wild boars (*Sus scrofa* spp.) that recently emerged in Asia. First described in Kenya in 1921 [1], ASF spread to countries in Western Europe during the mid-1950s but was painstakingly eliminated across the region with the exception of the island of Sardinia. ASF then made its way into Eastern Europe in 2007 via Georgia [2] before appearing in China in mid-2018, after which it infiltrated nearby Asian countries over the course of 2019 [3]. It is unclear how ASF entered China, but the circulating strain was genetically similar to the virulent strain of genotype II found in Georgia and Russia [4, 5]. Although the ASF virus (ASFV) does not infect humans, control of its spread is of immense international concern as domestic pigs are a valuable source of food and other commodities. Pork products account for 37% of global meat consumption [6], and products derived from pig parts are widely used in household and industrial applications, as well as for lifesaving medical treatments [7]. Currently, there are no treatments or effective vaccines available to combat ASF.

Nearly 100% fatality of infected pigs has resulted in biosecurity measures that include the immediate culling of all pigs at sites where ASFV is detected, as well as blanket depopulation within 3-km epidemic zones around infected units (e.g. farms, backyards). Following such measures, Chinese authorities reported culling around 1.2 million pigs between August 2018 and June 2019, and it was reported that in August 2019, there was a 37.9% decrease in the number of live pigs in China compared to the same time the previous year [3]. Unfortunately, the multifactorial nature of ASF transmission precludes culling alone from halting disease spread.

For the most part, ASF transmission between swine occurs through direct contact or aerosol routes, but the virus can also be transmitted via arthropod vectors, fomites, or consumption of infected pork-related products – typically through the practice of feeding pigs raw swill, which is food scraps or food waste that contains or has come into contact with meat or meat products [8]. Indeed, early epidemiological studies found that the spread of ASFV in China was associated with biosecurity breaches such as raw swill feeding, improper disposal of dead animals, contaminated vehicles and workers, and transport of live pigs and their products across regions [9, 10]. Armed with this knowledge, China banned the use of nonheated swill, disallowed swill feeding in provinces with ongoing outbreaks, set up inspection and disinfection stations to

© The Author(s), 2024. Published by Cambridge University Press. This is an Open Access article, distributed under the terms of the Creative Commons Attribution licence (<http://creativecommons.org/licenses/by/4.0>), which permits unrestricted re-use, distribution and reproduction, provided the original article is properly cited.

control farm traffic within 10-km buffer zones around the epidemic zones, limited the transportation of live pigs, closed and disinfected slaughterhouses in provinces with reported outbreaks, and closed live pig markets in affected and adjacent provinces [10, 11].

Identification of outbreak transmission events and development of effective control programmes remain works in progress for affected countries [8, 12], though it may be possible to develop more effective control programmes by re-evaluating the spatiotemporal configuration and directionality of transmission for potentially linked outbreaks. Although infector–infectee relationships between outbreaks are largely unestablished, it is possible to identify likely infector–infectee pairings between outbreaks by reconstructing transmission networks using temporal and spatial data outbreak data reported by China to the World Organization for Animal Health (WOAH). These data can also be used to quantify the transmissibility of ASF spread by calculating the reproduction number (R), which represents the average number of secondary infections caused by a single, primary infection. When R is < 1 , transmission is reduced and the number of infections decreases with each generation. Previous between-unit estimates of R during ASF outbreaks ranged from 2–3 between farms in Russia [13] to 1.6–3.2 between pig herds in Uganda [14].

In this study, we quantified factors of ASF transmission and surveillance over the course of the epidemic in China. First, we estimated the reporting delay – an indicator of how fast the outbreaks are being recognized by the authorities – and outbreak length – an indicator of how effectively each outbreak is managed. Next, we implemented four algorithms to reconstruct possible transmission networks and characterize the dynamics of ASF spread in China. This allowed us to examine changes in the ASF reproduction number over time as well as calculate the mean transmission distance and serial intervals (time between illness onset for pigs in infector–infectee paired units) of ASF in China. We restricted our analysis to the time period from the first report of ASF in China in August 2018 to September 2019. The latter date indicated the time when the data reporting became scarce. During the COVID-19 outbreaks and lockdowns of 2020–2023, the occurrence of ASF cases in China was greatly affected; for example, vehicle and person movement were severely restricted [15]. As of mid-2023, the real scale of ASF spread in China and Southeast Asian Region remains largely uncertain [16].

Methods

Epidemiological data

The data set of all ASFV-infected units was aggregated from publicly available immediate notifications and follow-up reports submitted by the Ministry of Agriculture and Rural Affairs of the People's Republic of China (MARA) [17] to WOAHA beginning in August 2018 and published in the World Animal Health Information System (WAHIS) [18]. An ASF outbreak was defined as at least one pig infected with ASFV within a single unit – either a farm, backyard, slaughterhouse, or village. In China, the detection of ASF triggers the establishment of an epidemic zone with a radius of 3 km around the infected unit within which all pigs are culled and entrance of live pigs is restricted by blockade. A 10-km buffer zone is also established, in which inspection and disinfection stations are set up to control traffic to and from the infected unit. Infected slaughterhouses were shut down and decontaminated, and MARA then tasked slaughterhouses with conducting self-inspection using laboratory tests [19]. Live pig trading markets in affected areas were

closed. Outbreaks related to infected units were declared over when there were no new infections within the epidemic zone for 6 weeks [20]. End-of-outbreak information was not retrospectively updated in the WAHIS reports, so we supplemented the data with dates retrieved from official announcements by MARA. If the dates obtained from WAHIS and MARA for the same outbreak differed, we used the earlier date. To assess the spatial correlation between the density of live pigs and the location of infected units, we used values of the global livestock population predicted by the Gridded Livestock of the World (GLW v3) system of the Food and Agriculture Organization (FAO) of the United Nations [21].

A total of 155 outbreaks were reported between 4 August 2018 and 9 September 2019, of which 152 were outbreaks among domestic pigs, two were outbreaks on wild boar farms in Heilongjiang and Inner Mongolia, and one was a report of a sole infected wild boar in Jilin Province. The wild boar was excluded from our analyses. We also disregarded six outbreaks reported in March, June, and August 2019 linked to the interception of transport vehicles carrying infected pigs. In the first two reports, transport trailers carrying 150 pigs (9 dead) and 32 pigs (1 dead) were intercepted at highway checkpoints for animal health supervision in Sichuan and Guizhou provinces and the origin of these pigs was uncertain [22]. Swine in the other four outbreaks in late August 2018 similarly had unknown origin. The exclusion of these reports resulted in a total of 148 outbreaks included for analysis.

Reporting delay

We defined reporting delay as the time between the date of outbreak start and the date of outbreak notification to WOAHA. Among the 148 outbreaks, only 135 included both the start and notification dates. We right-censored the records with an unspecified report date and assumed that the reporting date could be any time between one day after the start of the outbreak and the date of release of the report by WOAHA. We estimated the distribution of the reporting delay using a discretized probability distribution derived from the cumulative distribution functions $H(t; \alpha)$ of single gamma, log-normal, and Weibull distributions, and their mixtures. The probability an infected unit was reported at time t after infection is detected is modelled by $h_{t,\alpha} = H(t+1; \alpha) - H(t; \alpha)$. The parameter α represents a vector of the means and standard deviation (SD) of the distributions. In case of a mixture, the function $h_{t,\alpha}$ is decomposed into two discretized probability distributions as follows: $h_{t,\alpha} = \rho h_{t,\alpha_1} + (1-\rho)h_{t,\alpha_2}$, where ρ is the relative weight of the first distribution over the second ($0 < \rho < 1$); $\alpha = \{\alpha_1, \alpha_2, \rho\}$, $\alpha_i = \{\mu_i, \sigma_i\}$ consists of the mean (μ_i) and SD (σ_i) of the probability mass function h_{t,α_i} ($i = 1, 2$).

Reconstruction of probable transmission networks

We employed three transmission kernels f following nearest neighbour, exponential function, and equal probability algorithms [23–25] to reconstruct probable transmission networks of ASF in China. For each algorithm, f is dependent solely on the distance between paired units. For the nearest neighbour kernel, the unit closest to the infectee was selected as the infector. In contrast, the exponential and equal probability kernels have an exact functional form, such that the exponential kernel $f(i, j; \bar{d}) = \exp(-d_{ij}/\bar{d})$, where \bar{d} is the scale of the effective transmission distance, and the equal probability kernel $f(i, j; \bar{r}) = 1$ if $d_{ij} < \bar{r}$ and is 0 otherwise. The two kernels will produce an identical transmission network if $\bar{d}, \bar{r} \rightarrow +\infty$. For the equal probability algorithm, we set the probability of transmission as

equally likely within a given radius \bar{r} and zero otherwise. In our simulations, we set $\bar{r} = 3\bar{d}$, which is also approximately equal to the 95th percentile of the exponential kernel function. All algorithms restricted unit linkage to infector and infectee pairings where the estimated serial interval was longer than the ASF incubation period based on a gamma distribution with a mean of 6.3 days and an SD of 1.3 days [26].

Next, we assigned weights w_{ij} to each potential infector i and infectee j pairing. The value for each weight was set to the respective value of the kernel function $f(i, j | \circ)$ unless the following two conditions were violated: (i) the outbreak began at the infectee location later than it began at the infector location plus the estimated incubation period for ASF and (ii) the outbreak began earlier than it ended at the infector location minus the incubation period. Otherwise, the weight w_{ij} was set to zero. The incubation period distribution was given as a gamma distribution with a mean of 6.3 days and an SD of 1.3 days [26]. Imputed outbreak end dates ($n=2$, as in Figure 1b) were drawn from a gamma

distribution of all known outbreak start to end time intervals. Implementation of these two uncertainties resulted in a probabilistic non-uniqueness of the transmission network even when the linkage of an infector and an infectee was established using the nearest neighbour algorithm.

The transmission probabilities p_{ij} for each infectee were set by normalizing the weights for all potential infectors as follows: $p_{ij} = w_{ij} / \sum_{i=1 \dots N} w_{ij}$, $j = 1 \dots N$. The infectee is linked to a single infector by sampling from the categorical distribution:

$$i_{\leftarrow j} \sim \text{Categorical} \left(\mathbf{p} = \{p_{ij}\}; j = 1 \dots N \right).$$

When $p_{ij} \equiv 0$, the linkage of infectee to infector does not occur (e.g. the index outbreak).

We then estimated the mean transmission distance based on the methods developed by Salje et al. [27], which extends the temporal framework developed by Wallinga and Teunis [28] to include a spatial dimension. The temporal dimension is governed

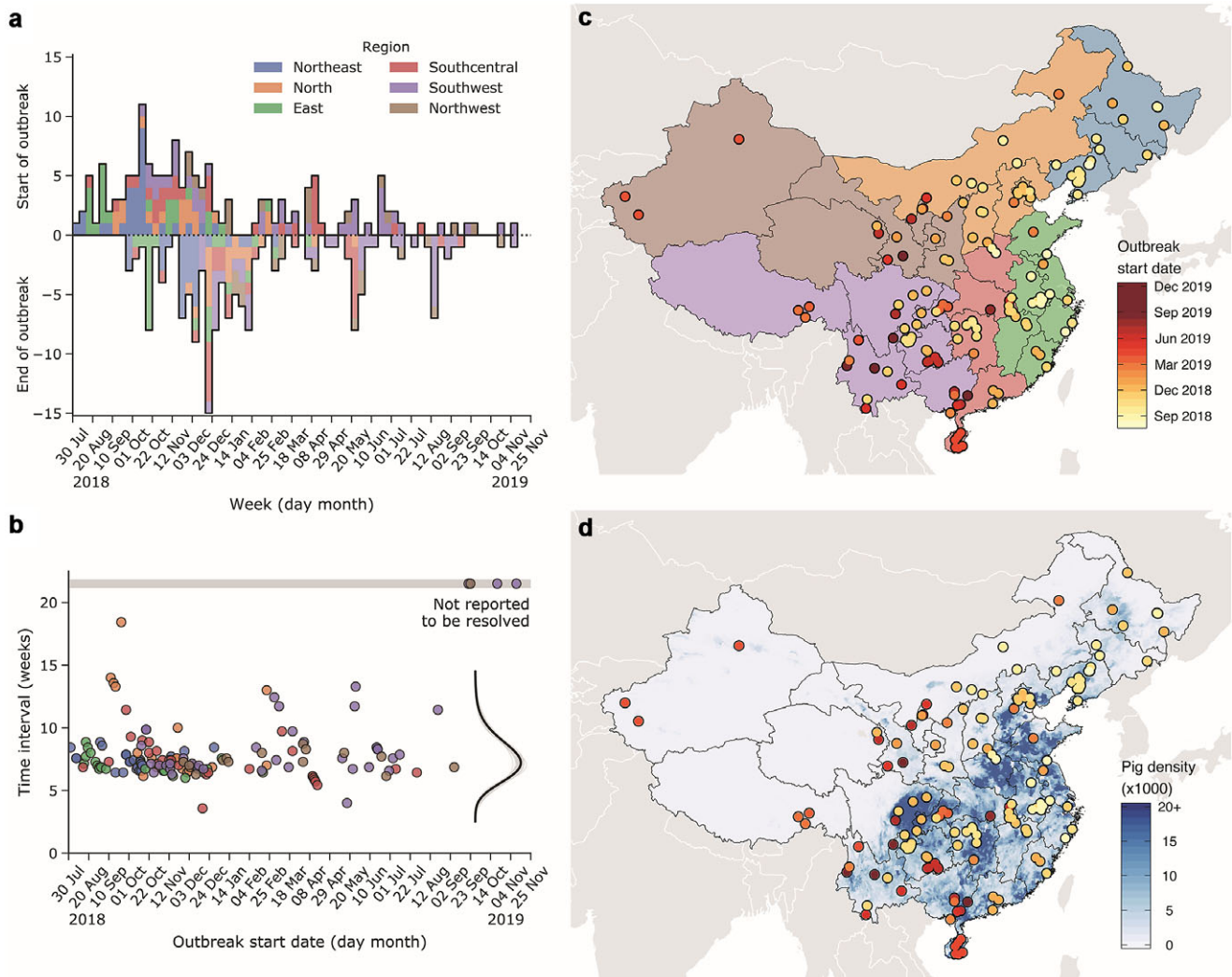


Figure 1. Characteristics of African swine fever (ASF)-infected farms in China from July 2018 to May 2019. (a) Weekly number of reported outbreaks by outbreak start and end dates for the six regions in China. (b) Time interval between the outbreak start and end dates by date of outbreak start. The point colours represent the region in which each infected unit is located, consistent with colours in (a). Points within the horizontal grey bar are unresolved cases. Inset in (b): The right-hand vertical line with grey shading indicates the distribution of the time interval and 95% credible intervals, respectively. The scale is not shown, but the area under the curve is equal to 1. (c) Geographical distribution and outbreak start date of ASF-infected farms. Point colours indicate the start date of outbreak in each infected unit. (d) Pig density and geographical location of ASF-infected unit. Point colours indicate the start date of outbreak and blue shade presents the density of lived pigs in China, as reported by the Food and Agriculture Organization (FAO).

by the generation time distribution, and the spatial dimension is characterized by a transmission kernel distribution, which describes the probability of observing two cases at a given distance. The generation time distribution was estimated separately using the data from previously documented ASF outbreaks [29, 30] by implementing a multi-generational framework [31–33] (Supplementary material S1).

We used a probability generation function $g(t; \theta_g)$, where the parameter set $\theta_g = \{\mu_g, \sigma_g\}$ consists of the mean μ_g and SD σ_g to describe the generation time distribution. The distribution was discretized by day following the form of $G(t; \theta_g) = \int_{t-1}^t g(\tau; \theta_g) d\tau$ ($t = 1, 2, \dots$). Next, we defined a Wallinga–Teunis matrix \mathcal{W} , where rows represent infectees i and columns represent potential infectors j . Each element of the matrix is a probability of transmission between i and j of

$$\mathcal{W} = \left\{ \frac{G(t_i - t_j; \theta_g)}{\sum_k G(t_i - t_k; \theta_g)}; 1 \leq i, j \leq N \right\}.$$

The infectee–infector pairings (i, j) were identified using sampling from a categorical distribution respective to the rows of the Wallinga–Teunis matrix: $\{\mathcal{W}_{ij}; j = 1, \dots, N\}$. If all elements in a row of the matrix \mathcal{W} appeared to be zero, the case was left unpaired (e.g. the index outbreak).

We then used categorical sampling to construct the transmission network \mathcal{Z} . For any pair of nodes i and j , we determined a set of network paths connecting them and recorded the number of links ζ_{ij} in each path. This procedure was done repeatedly over a large set of sampled transmission networks to form the set of counts $\mathbf{Z}_{ij} = \{\zeta_{ij}\}$. We then defined $\pi(\zeta; i, j)$ as the frequency of observing the number of links ζ between i and j in a set \mathbf{Z}_{ij} and applied the formula obtained by Salje et al. to estimate the mean transmission distance by taking it as equal to the SD of the transmission kernel:

$$\mu_d = \sigma_d = \frac{1}{N_\Sigma} \sum_{i,j} \sum_{\zeta \in \mathbf{Z}_{ij}} \frac{2d_{ij}}{\sqrt{2\pi\zeta} \pi(\zeta; i, j)}.$$

Here, d_{ij} is the geographic distance between i and j and N_Σ is the total number of observed pairs (i, j) .

For validation, we performed numerical simulations to quantify the effect of underascertainment on the estimated mean transmission distance we calculated using the spatiotemporal case-distribution method developed by Salje et al. [27]. In order to do so, we used the Animal Disease Spread Model (ADSM) – a stochastic, spatial, state-transition simulation model for the spread of highly contagious diseases in animals [34]. We used a sample population of pig farms provided by the developers for the default setting: 461 units were distributed over a circular area with a radius of 600 km. The model parameters were chosen to simulate a situation close to a real spread of ASF. We set the incubation period distribution to a gamma distribution with a mean of 6.3 days and an SD of 1.3 days [26]. The infectious period was assigned to a gamma distribution with a mean of 9.15 days and an SD of 1.92 days, but we approximated the generation time distribution, defined as a convolution of the incubation period distribution and infectiousness period distribution, using a gamma distribution with the resulting mean of 9.45 days (95% credible interval [CI]: 6.04–13.42 days) and SD of 2.30 days (95% CI: 1.23–3.50 days). The direct (within-pen) and indirect (between-pen) contact rates were set to 2.62 and 0.99, respectively [35]. As ASFV

is highly pathogenic, we set the probability of direct and indirect successful transmission to be 1.0. ADSM only considers the airborne transmission of the virus, which we modelled using an exponential decay function with an effective distance of 10 km. No control measures were considered in the simulations, which resulted in nearly 100% infection of the population.

Results

As of 9 September 2019, there were 148 outbreaks of ASF in China. All provinces in mainland China experienced at least one outbreak (Figure 1; Supplementary Figure S1). Outbreak units were classified as farms, backyard farms, villages, or slaughterhouses. The size of the pig population supported varied between and within unit types (Supplementary Figure S2). We found no significant correlation between outbreak start date and affected unit size (Pearson's $r = -0.044$, $N = 147$, $P = 0.589$) or type (ANOVA, $F(3,144) = 1.96$, $P = 0.123$), nor between the fraction of infected pigs and live pig density by province (Pearson's $r = -0.15$, $N = 147$, $P = 0.406$).

Reporting delay for the outbreaks had a mean of 7.6 weeks (95% CI: 7.3–7.8) and an SD of 1.6 weeks (95% CI: 1.5–1.8 weeks) (Figure 1b; Table 1). The distribution of the reporting delay displayed a heavy tail and bimodality (Supplementary Figure S3). We fit the reporting delay to a combination of lognormal (for shorter reporting delays) and gamma (for longer reporting delays) distributions, as this combination yielded the minimal median Watanabe–Akaike information criterion (WAIC) value (Table 2). The mean reporting delay assuming a shorter reporting delay (lognormal distribution) was 5.4 days (95% CI: 4.4–6.5 days) with an SD of 3.8 days (95% CI: 2.3–5.5 days), and the mean reporting delay assuming a longer reporting delay (gamma distribution) was 21.6 days (95% CI: 6.8–34.2 days) with an SD of 10.7 days (95% CI: 0–21.0 days). The mean reporting delay using the combined lognormal and gamma distributions was 6.3 days (95% CI: 5.5–7.2 days) with an SD of 5.3 days (95% CI: 4.1–6.7 days). There was no clear correlation found between reporting delay and unit type (ANOVA, $F(3,131) = 1.25$, $P = 0.293$) or unit size (Pearson's $r = -0.04$, $N = 134$, $P = 0.655$) (Supplementary Figure S2a,b).

Figure 2 shows the reconstructed transmission networks of ASF spread among infected units using nearest neighbour, exponential function, and equal probability algorithms, which rely on knowledge of the geographic location of reported outbreaks – see Methods section for details. We required that the time between paired outbreak start dates was no shorter than the ASF incubation period. The nearest neighbour algorithm yielded an estimated mean transmission distance of 332 km (95% CI: 213–1548 km) with a mean serial interval of 29.0 days (95% CI: 6–62 days)

Table 1. Fit of the time period between the start and the end of the outbreak to different distributions

Distribution	Mean, weeks	SD, weeks	WAIC
Gamma	7.6 (7.3–7.8)	1.6 (1.5–1.8)	565.5
Log-normal	8.1 (7.6–8.6)	3.1 (2.8–3.5)	618.0
Weibull	7.3 (6.9–7.6)	2.4 (2.2–2.6)	636.4

The mean and standard deviation (SD) of the probability mass function for each distribution are compared by relative values of the Watanabe–Akaike information criterion (WAIC) with 95% credible intervals shown in brackets.

Table 2. Fit of the reporting delay to different distributions

Distribution	μ_1 , days	σ_1 , days	μ_2 , days	σ_2 , days	ρ	WAIC
Mixture of log-normal (1) and gamma (2)	5.5 (4.4–6.5)	3.9 (2.4–5.5)	22.1 (8.4–35.0)	10.9 (0.1–21.7)	0.91 (0.77–1.00)	793.8
Single log-normal	6.3 (5.5–7.2)	5.3 (4.0–6.6)	–	–	–	797.6
Mixture of gamma (1) and log-normal (2)	4.4 (2.3–6.1)	3.0 (0.1–6.3)	11.1 (5.5–23.7)	9.8 (4.0–20.7)	0.49 (0.00–0.91)	799.1
Mixture of two gammas	4.9 (4.2–5.7)	2.8 (2.0–3.5)	18.7 (9.0–29.6)	10.8 (5.3–18.3)	0.85 (0.68–0.97)	799.4

Parameters μ_i and σ_i ($i = 1, 2$) represent the mean and standard deviation of the probability mass function for each distribution of the reporting delay by distribution type, ρ is the weight attributed to each configuration by the relative values of the Watanabe–Akaike information criterion (WAIC), and 95% credible intervals are shown in brackets. Although all possible combinations of single gamma, log-normal, Weibull distributions, and their mixtures were considered, only the top four configurations with minimal WAIC values are shown here.

between paired transmission events. The exponential function algorithm yielded a mean transmission distance of 456 km (95% CI: 22–1550 km) and a mean serial interval of 29.3 days (95% CI: 6–64 days) with the distance kernel set at $\bar{d} = 200$ km. Due to the time constraints we imposed (Section 2.3) or when the distance between an infectee and a potential infector exceeded the minimally allowed one, \bar{d} , we were unable to link an average of eight outbreaks (95% CI: 5–12) to any potential infector for these two methods (Supplementary Figure S4a,b).

The equal probability algorithm yielded a mean transmission distance of 344 km (95% CI: 23–595 km) and a mean serial interval of 29.5 days (95% CI: 6–64 days) with the effective distance set at 600 km, which is the 95th percentile of the previous kernel function. An average of 30 outbreaks (95% CI: 28–34; Supplementary Figure S4c,d) could not be linked to any potential infector due to the constraint on long-range transmission imposed by setting the effective transmission distance at 600 km. We performed sensitivity analyses for effective transmission distance used in the exponential function and equal probability algorithms, but did not find that either algorithm was sensitive to the value of the effective transmission distance (Supplementary Figures S5, S6).

Our use of the spatiotemporal case-distribution algorithm developed by Salje and colleagues [27] resulted in a mean transmission distance of 483 km (95% CI: 449–503 km). A variation in the mean (range 1–14 weeks) and SD (range 1–7 weeks) of the generation time distribution led to the approximate range of the mean transmission distance between 200 and 500 km (Figure 3). The mean transmission distance tended to increase if either the mean or SD of the generation time were increasing.

Additional numerical simulations of a virtual outbreak of ASF using ADSM (see Methods section) revealed that the removal of a fraction of reported cases with both temporal and spatial information led to a substantial overestimation of the mean transmission distance. A sample run over 129 days resulted in infection of 440 out of 461 virtual swine farms (Figure 4a,b). The estimated mean transmission distance without any underascertainment was 58 km, thereby confirming that the removal of geographic information for even a large fraction of cases does not affect the obtained estimate [27] – see dashed orange in Figure 4c. However, we also found that the complete removal of outbreaks from the data set results (reflecting underascertainment of incidence of infection) resulted in a substantial overestimation of the mean transmission distance – see solid blue in Figure 4c. We thus argue that the underascertainment of cases may significantly contribute to

the overestimation of the mean transmission distance when using the spatiotemporal case-distribution algorithm developed by Salje and colleagues.

Discussion

ASFV has remained in circulation in China years after it was first detected. Our study used mathematical modelling to quantify ASF transmission within China. Whereas various recent studies [36, 37] primarily focused on assessing the spread of ASF in Europe, only few addressed the spread in China [38]. However, the ASF spread in China has increasingly been recognized to have global economic consequences [39] and a better understanding of ASF transmission dynamics, as investigated in the current study and other recent publications [38, 40], is critical to the development of control policies. We found that the median serial interval was approximately 29 days and the mean distance between suspected transmissions ranged from 332 to 456 km, reflecting the wide temporospatial spread of the epidemic in China. These results suggest that 1) swine husbandry practices and production systems that lend themselves to long-range transmission drove ASF spread and 2) outbreaks went undetected by the surveillance system.

The initial reduction of the ASF reproduction number below the threshold value of 1 for our three geographically based algorithms coincided with official reports of successful outbreak control measures in November 2018. However, persistent transmission led to sporadic increases in the reproduction number later in 2019. The swiftest decline in the reproduction number occurred following the nearest neighbour algorithm, while the exponential and equal probability models exhibited smoother, transient dynamics. Having now been detected in many countries in Asia, ASF has become a critical international biosecurity concern and our estimates of the weekly reproduction number, serial interval, and transmission distance of ASF in China can help inform intervention and management strategies.

Outbreak underascertainment is the main limitation of our study. It is plausible that ASF surveillance capacity in China was not sensitive enough to detect all infections – particularly in smaller units with lower biosecurity – leading to the underascertainment of outbreaks and consequently underestimation of the reproduction number with the methods we used. Several other factors may contribute to this situation, including the incentives of local authorities to conceal ASF outbreaks in order to minimize reputational damage; see pages 5–6 in [15]. We suspect that the large estimates of the mean

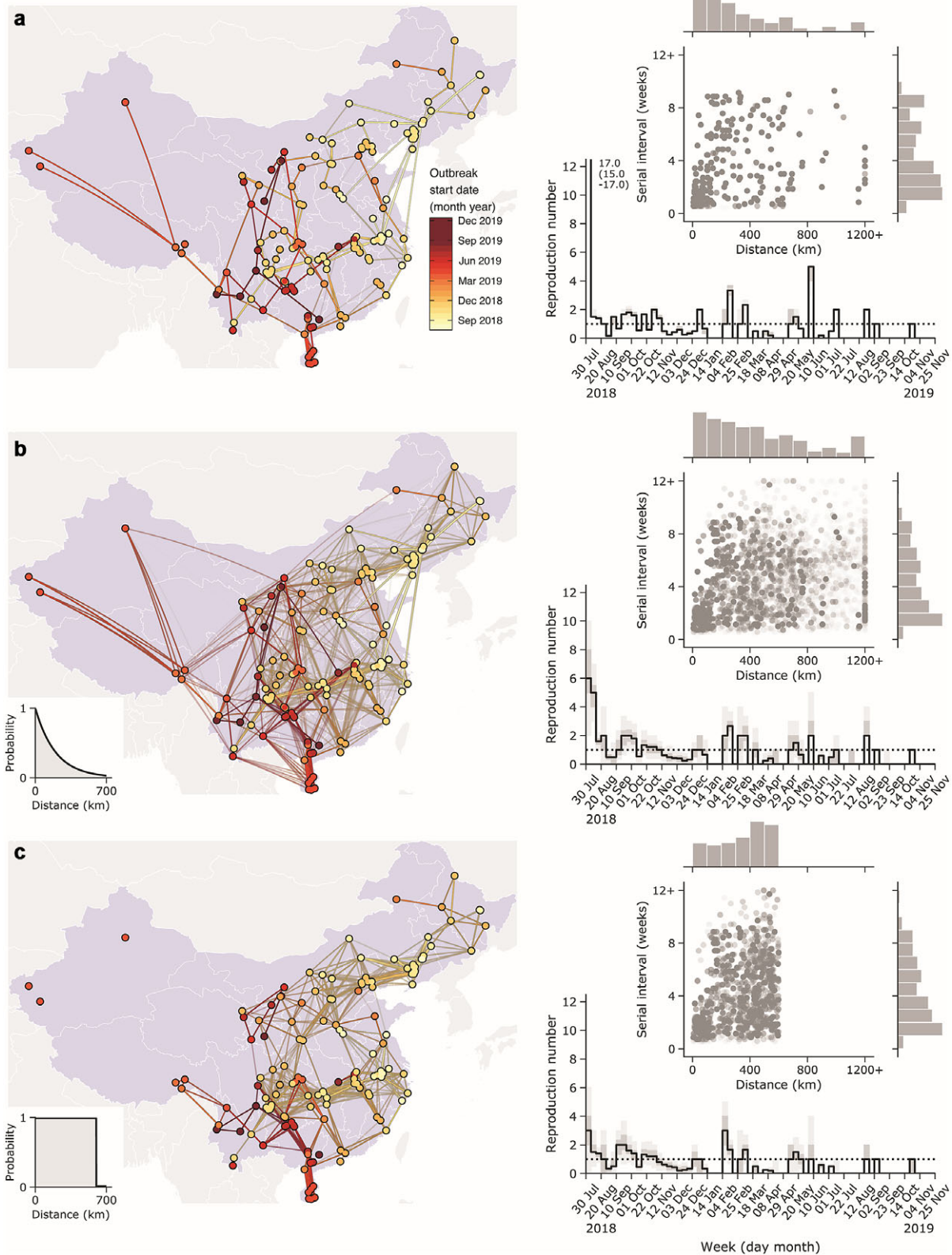


Figure 2. Reconstructed transmission networks of African swine fever (ASF) outbreak from July 2018–September 2019 in China and estimates of reproduction number and serial interval from reconstructed networks. Three transmission networks are reconstructed by using (a) nearest neighbour, (b) exponential function, and (c) equal probability algorithms, analysing only outbreaks reported to the World Organization for Animal Health (WOAH). The dot and line colours in the map represent the start date of the outbreak in each infected unit. Correlations between the serial interval and transmission distance are shown in the upper right side of each figure. The points indicate each ASF-infected farm and bars represent the distribution of estimated distance and serial intervals, using the reconstructed transmission networks, respectively. The lines and shades in each of the figures on the right show the estimated reproduction number and its 95% credible intervals by calendar week. The epidemic threshold ($R = 1$) is represented with a dashed line.

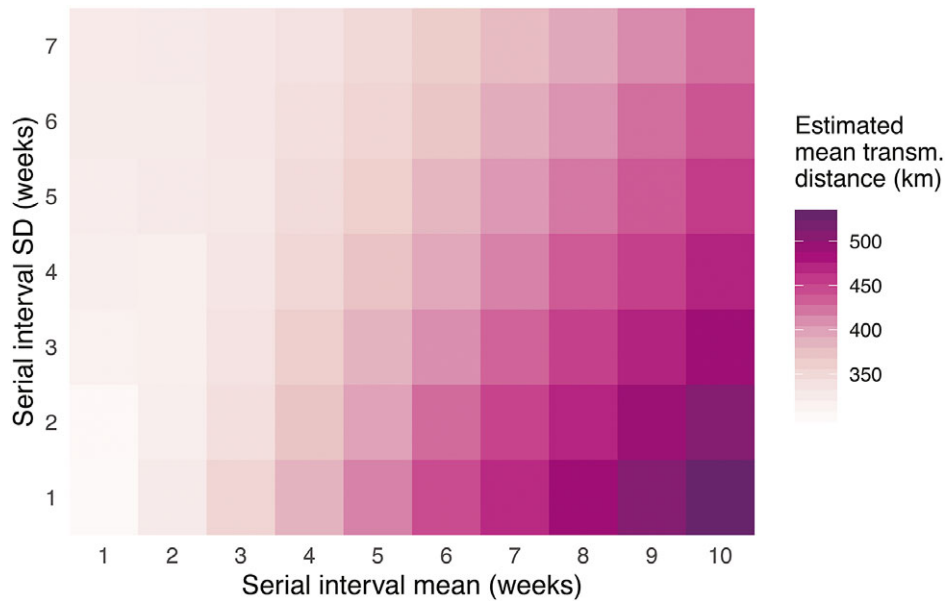


Figure 3. Mean transmission distance based on varying mean and standard deviation (SD) values of the serial interval distribution. Estimation relies on a generalized Wallinga–Teunis method developed by Salje and et al. [27]. Both the spatial transmission kernel and serial interval are assumed to follow a normal distribution, with 1000 simulations of the transmission networks used for each particular value of the mean and SD. For additional details, see the Methods section.

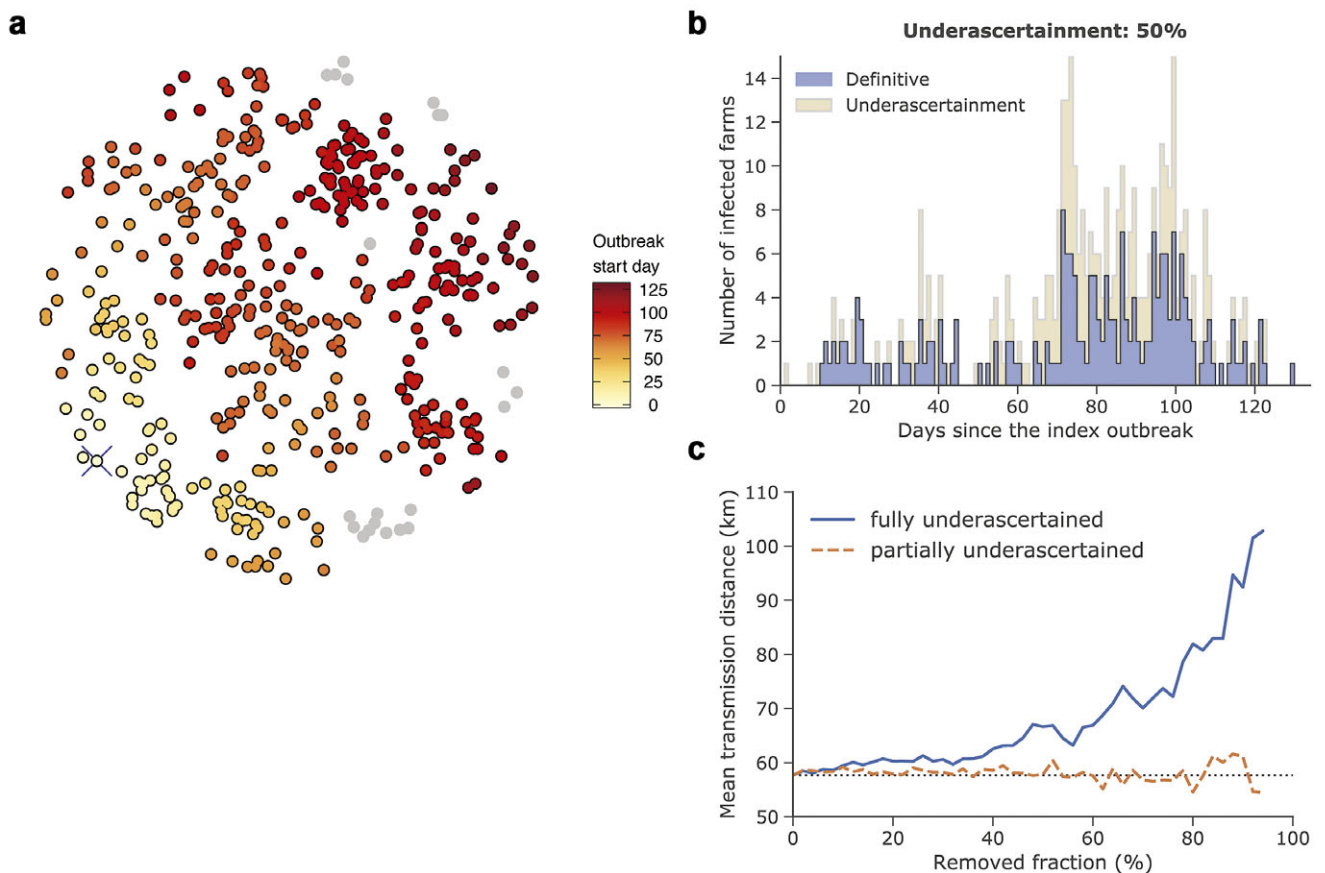


Figure 4. Simulated outbreak of ASF using Animal Disease Spread Model (ADSM) [34]. (a) shows the spatiotemporal spread of the disease. The crossed yellow dot in the bottom left-hand side of the circle is the index case. Grey points represent uninfected farms. (b) depicts the epidemic curve. The dark bars represent definitive (reported) cases and the light bars represent partially or fully underascertained cases – that is, cases missing spatial (geolocation) information or unreported cases that are missing both spatial and temporal information. (c) Estimation of the mean transmission distance for fully underascertained cases (solid line) or partially underascertained cases (dashed line). The dotted horizontal line is the estimate for the data set with no underascertainment.

transmission distance could be a consequence of the underascertainment of infected units. The estimates of the mean transmission distance using the spatiotemporal case-distribution method were also larger than anticipated. This was likely due to the underascertainment of infected units or the intentional culling of susceptible pigs within the epidemic zones surrounding the reported units. Both factors would reduce the number of susceptible pigs within a shorter transmission distance, therefore making transmission of ASF to new regions possible only through long-range transmissions and prolonged generation intervals. Although we investigated the possible impact of outbreak underascertainment on transmission distance using simulation data, there are still some methodological uncertainties when both temporal and spatial information is missing. If the true degree of underascertainment can be estimated (e.g. using genetic data or environmental sampling), the ASF reproduction number could be more accurately assessed.

Compared to outbreaks in other regions, such as Western Europe or the Korean peninsula, wild boars played a relatively minor role in the spread of ASF in China. Only two outbreaks were reported by the WOAHP concerning wild boar farms, and one report concerned an infected wild boar during the study period. Ticks and wild boars have only been mentioned in a few Chinese articles as potential carriers of ASF to domestic pigs [41]. In the light of this, we do not believe our lack of consideration for transmission among wild boars to be a limitation.

We also did not consider the importation of ASFV from outside of China and only modelled within-country transmission. This could perhaps be accomplished using other data, but it is beyond the scope of this study. We also did not fully consider the impact of the Lunar New Year – one of the biggest holidays in China – in our calculations of the reporting delays and outbreak lengths. However, we could not find any clear correlation between the submission delay (i.e. time interval between the notification date of the outbreak in the Chinese government and the report submission date to WOAHP) and the official dates of the holiday.

Control of ASF in China, the world's leading producer and consumer of pork [42], is of critical importance to countries that import Chinese pig products as the virus may remain viable in blood and tissues for long periods of time [43, 44]. Although vaccines for ASF are under development [45], biosecurity-based control measures remain key to preventing the transboundary spread of ASF, and a better understanding of the transmission distances and transmissibility of ASF in China can help inform management strategies to prevent further spread. The disease poses an ongoing threat to livelihoods and national swine-related gross domestic product, as well as to the development of important medical, industrial, and household products.

Although China has endeavoured to contain the spread of ASF, the economic implications of the outbreak have begun to show [39, 46]. Chinese import of pork from the United States is well above 2018 levels [47], and continued transmission of ASF may contribute to shortages of the lifesaving drug heparin, which is mainly produced by Chinese companies from porcine mucosa [7]. The various transmission pathways for ASF and inherent biosecurity risks and economic devastation to small-scale farms remain a persistent concern for China and neighbouring countries. After examining four algorithms to assess transmission pathways, we found a large mean transmission distance and lengthy serial intervals, which are likely due to the underascertainment of cases and a prevalence of long-range transmission events. Our results indicate that continued monitoring of transmission, improvements to surveillance across large distances and lengthy time periods, and increased biosecurity measures are

critical to the elimination of ASF in China. As well, it is important for China and other countries to consider all possible modes of transmission when developing biosecurity protocols, as wild boar reservoirs and arthropod vectors may further complicate transmission networks. Restructuring of biosecurity protocols is vital to containment of the threat at national and international levels.

Supplementary material. The supplementary material for this article can be found at <https://doi.org/10.1017/S0950268824000086>.

Data availability statement. All data used for this study can be found at <http://github.com/aakhmetz/ASF-in-China-2018-2019>.

Author contribution. Conceptualization: A.A., H.N.; Investigation: A.A., B.Y., S-m.J., H.N.; Methodology: A.A., S-m.J., H.N.; Visualization: A.A.; Writing – original draft: A.A., S-m.J., H.N.; Writing – review & editing: A.A., B.Y., H.L., Y.Y., N.M.L., S-m.J., H.N.; Data curation: H.L., N.M.L., S-m.J.; Formal analysis: H.L., Y.Y., N.M.L.; Funding acquisition: H.N.

Funding statement. H.N. received funding from the Health and Labour Sciences Research Grants (20CA2024, 20HA2007, 21HB1002, 21HA2016, and 23HA2005), the Japan Agency for Medical Research and Development (JP23fk0108685 and JP23fk0108612), the JSPS KAKENHI (21H03198 and 22K19670), the Environment Research and Technology Development Fund (JPMEERF20S11804) of the Environmental Restoration and Conservation Agency of Japan, Kao Health Science Research, the Daikin GAP Fund of Kyoto University, and the Japan Science and Technology Agency SICORP programme (JPMJSC20U3 and JPMJSC2105) and RISTEX programme for Science of Science, Technology and Innovation Policy (JPMJRS22B4). The funders had no role in the study design, data collection and analysis, decision to publish, or preparation of the manuscript. We thank the local governments, public health centres, and institutes for surveillance for assistance with laboratory testing, epidemiological investigations, and data collection.

Competing interest. The authors declare none.

Ethical standard. The present study used publicly available data and thus did not require ethical approval.

References

- [1] **Montgomery RE** (1921) On a form of swine fever occurring in British East Africa (Kenya Colony). *Journal of Comparative Pathology and Therapeutics* **34**, 159–191.
- [2] **Khomenko S**, et al. (2013) African swine fever in the Russian federation: risk factors for Europe and beyond. *EMPRES Watch* **28**, 1–14.
- [3] **Food and Agriculture Organization of the United Nations (FAO)** ASF situation in Asia update. Available at https://web.archive.org/web/20190406091517/http://www.fao.org/ag/againfo/programmes/en/empres/ASF/Situation_update.html (accessed 6 April 2019).
- [4] **Costard S**, et al. (2013) Epidemiology of African swine fever virus. *Virus Research* **173**, 191–197.
- [5] **Zhou X**, et al. (2018) Emergence of African swine fever in China, 2018. *Transboundary and Emerging Diseases* **65**, 1482–1484.
- [6] **Food and Agriculture Organization of the United Nations (FAO)** Meat consumption. Available at <https://web.archive.org/web/20190418181601/http://www.fao.org/ag/againfo/themes/en/meat/background.html> (accessed 18 April 2019).
- [7] **Vilanova E**, et al. (2019) Imminent risk of a global shortage of heparin caused by the African swine fever afflicting the Chinese pig herd. *Journal of Thrombosis and Haemostasis* **17**, 254–256.
- [8] **European Food Safety Authority (EFSA)**, et al. (2018) Epidemiological analyses of African swine fever in the European Union. *EFSA Journal* **16**, 106.
- [9] **Ministry of Agriculture and Rural Affairs of the People's Republic of China (MARA)** Where does African swine fever come from? How is it spread? Available at https://web.archive.org/web/20230117135608/http://www.moa.gov.cn/ztzl/fzzwfk/rdgz/201812/t20181212_6164823.htm (accessed 6 August 2023).

- [10] Wang T, et al. (2018) African swine fever: an unprecedented disaster and challenge to China. *Infectious Diseases of Poverty* **7**, 111.
- [11] Ministry of Agriculture and Rural Affairs of the People's Republic of China (MARA) Notice on Strengthening the Supervision and Administration of Live Pigs and Their Products. Available at https://web.archive.org/web/20190314124319/http://www.moa.gov.cn/govpublic/SYJ/201809/t20180925_6158459.htm (accessed 12 April 2009).
- [12] Miller RS, et al. (2019) Prospects for improving management of animal disease introductions using disease-dynamic models. *Journal of Animal Science* **97**, 2291–2307.
- [13] Gulenkin VM, et al. (2011) Cartographical analysis of African swine fever outbreaks in the territory of the Russian Federation and computer modelling of the basic reproduction ratio. *Preventive Veterinary Medicine* **102**, 167–174.
- [14] Barongo MB, et al. (2015) Estimating the basic reproductive number (R0) for African swine fever virus (ASFV) transmission between pig herds in Uganda. *PLoS ONE* **10**, e0125842.
- [15] Gale F, et al. How China's African Swine Fever outbreaks affected global pork markets. U.S. Department of Agriculture: Economic Research Service 2023; Economic Research Report No. ERR-326.
- [16] Normile D (2023) African swine fever settles into Asia. *Science News* 25 April.
- [17] Ministry of Agriculture and Rural Affairs of the People's Republic of China (MARA). Available at <http://www.moa.gov.cn> (accessed 6 August 2023).
- [18] World Animal Health Information System (WAHIS). Available at <https://wahis.woah.org/#/home> (accessed 6 August 2023).
- [19] Ministry of Agriculture and Rural Affairs of the People's Republic of China (MARA) (2019) Notice on printing and distributing the emergency implementation plan for African swine fever (2019 Edition). Available at http://www.moa.gov.cn/gk/tzgg_1/tz/201901/t20190129_6170838.htm (accessed 6 August 2023).
- [20] Ministry of Agriculture and Rural Affairs of the People's Republic of China (MARA) African swine fever. Notice of technical specifications. Available at http://www.moa.gov.cn/nygb/2015/shierqi/201712/t20171219_6104138.htm (accessed 6 August 2023).
- [21] Food and Agriculture Organization of the United Nations (FAO). Available at <https://www.fao.org/livestock-systems/en/> (accessed 4 April 2019).
- [22] Guang'an Municipal People's Government People's Republic of China. Available at http://www.guang-an.gov.cn/gasrmzfw/qxsd/2019-03/13/content_dd52e17f8401462b9bd9646069714715.shtml (accessed 6 August 2023).
- [23] Kraemer MU, et al. (2017) Spread of yellow fever virus outbreak in Angola and the Democratic Republic of the Congo 2015–16: a modelling study. *Lancet Infectious Diseases* **17**, 330–338.
- [24] Riley S, et al. (2015). Five challenges for spatial epidemic models. *Epidemics* **10**, 68–71.
- [25] Viboud C, et al. (2006) Synchrony, waves, and spatial hierarchies in the spread of influenza. *Science* **312**, 447–451.
- [26] Olesen AS, et al. (2017) Transmission of African swine fever virus from infected pigs by direct contact and aerosol routes. *Veterinary Microbiology* **211**, 92–102.
- [27] Salje H, et al. (2016) Estimating infectious disease transmission distances using the overall distribution of cases. *Epidemics* **17**, 10–18.
- [28] Wallinga J, et al. (2004) Different epidemic curves for severe acute respiratory syndrome reveal similar impacts of control measures. *American Journal of Epidemiology* **160**, 509–516.
- [29] Korennoy FI, et al. (2017) Estimating the basic reproductive number for African swine fever using the Ukrainian historical epidemic of 1977. *Transboundary and Emerging Diseases* **64**, 1858–1866.
- [30] SSI VNIIVViM (2014) The report on the ways of introduction and spread of ASF in the Odessa oblast in 1977.
- [31] Akhmetzhanov AR, et al. (2018) Real time forecasting of measles using generation-dependent mathematical model in Japan, 2018. *PLoS Currents* **10**, ecurrents.outbreaks.3cc277d133e2d6078912800748dbb492.
- [32] Yuan B, et al. (2019) Assessing dengue control in Tokyo, 2014. *PLoS Neglected Tropical Diseases* **13**, e0007468.
- [33] Worden L, et al. (2020) Measles transmission during a large outbreak in California. *Epidemics* **30**, 100375.
- [34] Harvey N, et al. (2007) The North American animal disease spread model: a simulation model to assist decision making in evaluating animal disease incursions. *Preventive Veterinary Medicine* **82**, 176–197.
- [35] Hu B, et al. (2017) Bayesian inference of epidemiological parameters from transmission experiments. *Scientific Reports* **7**, 16774.
- [36] Picault S, et al. (2022) The African swine fever modelling challenge: objectives, model description and synthetic data generation. *Epidemics* **40**, 100616. <https://doi.org/10.1016/j.epidem.2022.100616>
- [37] Sauter-Louis C, et al. (2021) African swine fever in wild boar in Europe—a review. *Viruses* **13**, 1717.
- [38] Ito S, et al. (2022) The evolution of African swine fever in China: a global threat? *Frontiers in Veterinary Science* **9**, 828498. <https://doi.org/10.3389/fvets.2022.828498>
- [39] Mason-D'Croz D, et al. (2020) Modelling the global economic consequences of a major African swine fever outbreak in China. *Nature Food* **1**, 221–228.
- [40] Li J, et al. (2022) Data-driven dynamical modelling of the transmission of African swine fever in a few places in China. *Transboundary and Emerging Diseases* **69**, e646–658.
- [41] Chen J, et al. (2022) Risk factors for the spread of African swine fever in China: a systematic review of Chinese-language literature. *Transboundary and Emerging Diseases* **69**, e1289–e1298.
- [42] United States Department of Agriculture Foreign Agricultural Service (USDA) Livestock and poultry: world markets and trade. Available at https://apps.fas.usda.gov/psdonline/circulars/livestock_poultry.pdf (accessed 6 August 2023).
- [43] Plowright W, et al. (1967) The stability of African swine fever virus with particular reference to heat and pH inactivation. *Archiv für die gesamte Virusforschung* **21**, 383–402.
- [44] Sindryakova IP, et al. (2016) The influence of temperature on the Russian isolate of African swine fever virus in pork products and feed with extrapolation to natural conditions. *Sel'skokhozyaistvennaya Biol* **51**, 467–474. <https://doi.org/10.15389/agrobiology.2016.4.467rus>
- [45] Barasona JA, et al. (2019) First oral vaccination of Eurasian wild boar against African swine fever virus genotype II. *Frontiers in Veterinary Science* **6**(137), 1–10.
- [46] You S, et al. (2021) African swine fever outbreaks in China led to gross domestic product and economic losses. *Nature Food* **2**, 802–808.
- [47] Sánchez EG, et al. (2019) Development of vaccines against African swine fever virus. *Virus Research* **265**, 150–155.